ACS APPLIED MATERIALS & INTERFACES

Research Article

www.acsami.org

Solution-Processed PEDOT:PSS/Graphene Composites as the Electrocatalyst for Oxygen Reduction Reaction

Miao Zhang, Wenjing Yuan, Bowen Yao, Chun Li,* and Gaoquan Shi

Department of Chemistry and Key Laboratory of Bioorganic Phosphorus Chemistry and Chemical Biology (Ministry of Education), Tsinghua University, Beijing 100084, China

Supporting Information

ABSTRACT: Composites of poly(3,4-ethylenedioxythiophene):poly(styrenesulfonate) (PEDOT:PSS) and reduced graphene oxide (rGO) have been prepared by solution mixing and applied as electrocatalysts for oxygen reduction reaction (ORR) after treatment with concentrated H_2SO_4. The blending of rGO induces the conformational change of PEDOT chains from benzoid to quionoid structure and charge transfer from rGO to PEDOT. H_2SO_4 post-treatment can remove part of insulating PSS from the surface of the PEDOT:PSS/rGO composite film, resulting in a significant conductivity enhancement of the composite. This synergistic effect makes the H_2SO_4-treated PEDOT:PSS/rGO composite a promising catalyst for ORR. It exhibits enhanced electrocatalytic activity, better tolerance to a methanol crossover effect and CO poisoning, and longer durability than those of the platinum/carbon catalyst.

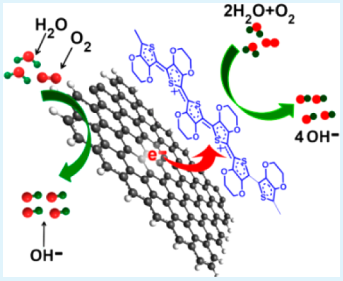

KEYWORDS: *poly(3,4-ethylenedioxythiophene):poly(styrenesulfonate), reduced graphene oxide, composite, oxygen reduction reaction*

1. INTRODUCTION

Oxygen reduction reaction (ORR) at the cathodes of fuel cells or metal−air batteries plays a key role on their electrochemical performances.[1−7] Platinum (Pt) and its alloy are known to be the best ORR catalysts.[1,3,8−10] However, commercialization of these catalysts has been greatly precluded by the prohibitive cost of Pt and their weak durability caused by agglomeration and/or CO poisoning and a methanol crossover effect.[8−10] Recently, metal-free ORR electrocatalysts have been widely explored for replacement of Pt-based catalysts because of their low cost, high activity, enhanced stability, and improved fuel tolerance.[11−21] An impressive example is poly(3,4-ethylenedioxythiophene) (PEDOT), an intrinsically conductive polymer (ICP), prepared by vapor-phase polymerization with high conductivity, improved structural ordering, and stability, that exhibited competitive activity and improved durability over Pt nanoparticles for ORR.[22] Heteroatom [nitrogen (N), sulfur (S), boron, and phosphorus]-doped or co-doped carbon (C) materials also showed excellent electrocatalytic performances for ORR.[13−20] One of the pioneering works was carried out by Dai and co-workers.[23,24] They reported that N-doped C nanotubes and graphene had high electrocatalytic activity for ORR with enhanced durability. Inspired by these findings, much effort has been devoted to this field and great progress has been achieved.[13−16] Nevertheless, some major challenges still retain on the way to the practical applications of these metal-free catalysts. Particularly, the preparation of these ICP and/or C-based catalysts usually requires rigorous reaction conditions, tedious procedures, and special instruments.[11−16] Thus, the development of a new type of metal-free ORR catalysts under mild conditions is still extremely desirable and can be considered to be one of the highest priorities in the development of fuel cells and metal−air batteries.

As part of our interest in the development of metal-free ORR catalysts,[25−27] herein, we report a facile method for the preparation of ORR catalysts through mixing of aqueous suspensions of commercially available PEDOT:poly(styrenesulfonate) (PEDOT:PSS) and reduced graphene oxide (rGO), followed by treatment of the drop-casted composite films with concentrated H_2SO_4. The design rationale for the composite catalyst is illustrated in Figure 1. PEDOT:PSS chains can be assembled onto the surfaces of rGO sheets through π-stacking interactions between both components.[28−30] Hybridization of PEDOT:PSS with rGO and the subsequent treatment with H_2SO_4 can significantly increase the electrical conductivity of PEDOT because of alternation of the PEDOT resonating ground states through strong $\pi-\pi$ interaction and segregation and partial removal of PSS chains from PEDOT:PSS.[31,32] On the other hand, the positively charged PEDOT backbones have electron-withdrawing ability to create net positive charges on rGO sheets via intermolecular charge transfer. This case is similar to the previously reported composites of positively charged poly(diallyldimethylammonium chloride) (PDDA) and C nanotubes or rGO.[33,34] It was proposed that the positively charged C atoms on rGO sheets induced by PDDA facilitate O_2 adsorption and also can readily attract electrons from the anode to accelerate ORR.[33,34] Accordingly, the resultant PEDOT:PSS/rGO composite films are expected to exhibit

Received: December 16, 2013
Accepted: January 24, 2014
Published: January 24, 2014

   dx.doi.org/10.1021/am405771y | ACS Appl. Mater. Interfaces 2014, 6, 3587−3593

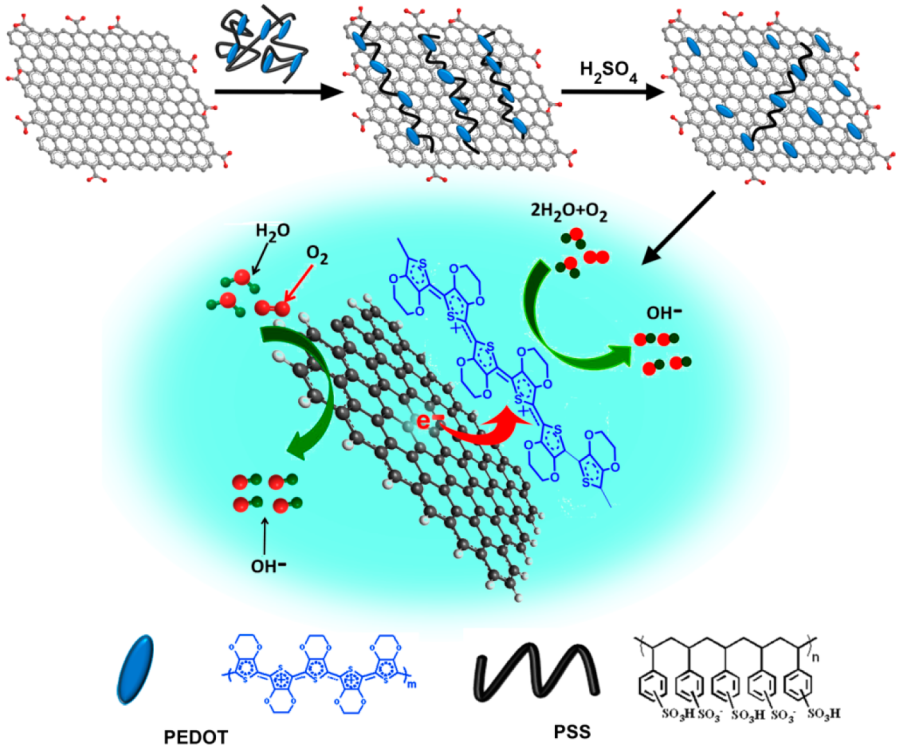

Figure 1. Schematic illustration of the preparation of a PEDOT:PSS/rGO composite and the design rationale for ORR.

synergistically enhanced electrocatalytic activity for ORR. Furthermore, the solution-processing method developed here has merits of mild conditions, excellent amenability to operation, and scalability for industrial utilization.

2. RESULTS AND DISCUSSION

Structures of the PEDOT:PSS/rGO Composites. The morphologies of rGO and the PEDOT:PSS/rGO composite were investigated by transmission electron microscopy (TEM) and atomic force microscopy (AFM). rGO sheets have smooth surfaces with slight wrinkles (Figure 2a). On the other hand, the PEDOT:PSS/rGO composite has a homogeneous sheetlike structure with granular PEDOT:PSS distributed on rGO surfaces (Figure 2b). AFM images show that the rGO sheets have an average thickness of 0.9 nm (Figure 2c), whereas the PEDOT:PSS/rGO composite sheet has an average thickness of around 5.0 nm (Figure 2d), indicating that PEDOT:PSS was noncovalently functionalized on the surface of the rGO nanosheet.[28−30]

Raman spectroscopy was employed to study the changes that occurred at the molecular level upon interaction between PEDOT:PSS and rGO. As shown in Figure 3a, the pristine PEDOT:PSS exhibits a prominent peak at 1444 cm^{-1}, corresponding to the C_α═C_β symmetrical stretching vibration of the five-membered thiophene rings.[35] Upon mixing with rGO, this peak is red-shifted to 1433 cm^{-1}. It is known that PEDOT has two resonant structures of benzoid and quinoid in the ground state, in which the benzoid structure is favored for a coil conformation, whereas the quinoid structure is characteristic of a linear or expanded coil structure.[36] Thus, it is reasonable to conclude that the introduction of rGO induced the conformational change of PEDOT chains from benzoid to quionoid structure because of the strong π-stacking interactions between PEDOT and the rGO basal plane. This intermolecular interaction was also supported by monitoring the Raman

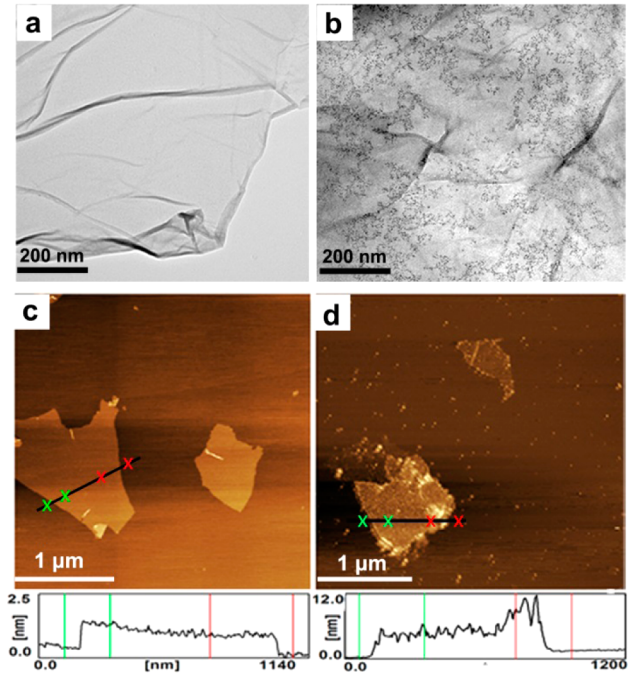

Figure 2. TEM (a and b) and AFM (c and d) images of rGO (a and c) and the PEDOT:PSS/rGO composite (b and d).

spectral changes of rGO before and after mixing with PEDOT:PSS because the G band of rGO is sensitive to intermolecular charge transfer.[34] As expected, rGO displays two dominant peaks at 1348 and 1592 cm^{-1}, which correspond to the D and G bands, respectively.[37,38] Upon mixing rGO with PEDOT:PSS, the G band of rGO is blue-shifted by 8 cm^{-1}, indicating intermolecular electron transfer from rGO to PEDOT. Charge transfer will create net positive charges at

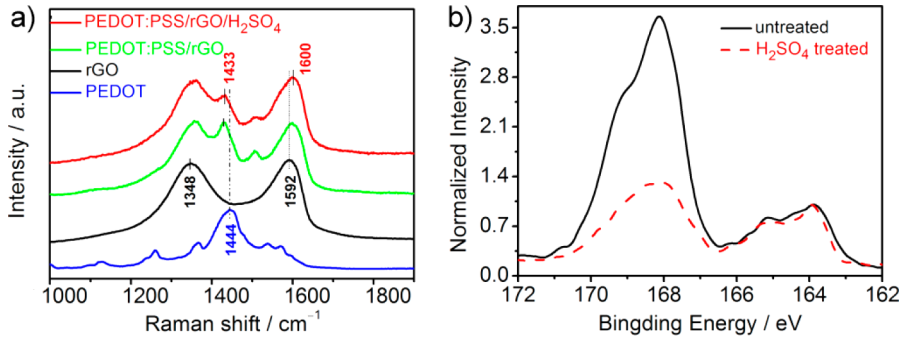

Figure 3. (a) Raman spectra of PEDOT:PSS, rGO, and PEDOT:PSS/rGO composites before and after treatment with concentrated H_2SO_4. (b) S 2p XPS spectra of PEDOT:PSS/rGO films before and after treatment with concentrated H_2SO_4.

the C atoms of the rGO sheets of the composite, facilitating its electrocatalysis of ORR.[33,34]

The Raman spectral features of PEDOT and rGO in the composite are scarcely changed upon treatment with concentrated H_2SO_4. To further elucidate the composition changes of the PEDOT:PSS/rGO composite upon this post-treatment, X-ray photoelectron spectroscopy (XPS) spectra of PEDOT:PSS/rGO before and after H_2SO_4 treatment were recorded (Figure 3b). The S 2p peak with a binding energy of 168.1 eV is the S signal from PSS, whereas those at 163.9 and 165.0 eV are the S 2p bands of the S atoms from PEDOT.[32] The intensity ratios of the S 2p peaks related to PEDOT and PSS increased from 1:2.88 to 1:1.16 after H_2SO_4 treatment, signifying removal of about 59% PSS from the film surface. Thus, the significant conductivity enhancement of the composite upon H_2SO_4 treatment is attributed to partial removal of the PSS component from the composite film (Figure S1 in the Supporting Information, SI). It is also clear that the loss of PSS from the PEDOT:PSS/rGO composite is less than that of PEDOT:PSS (Figure S2 in the SI). This is possibly due to the strong interaction between PSS and rGO, thus suppressing removal of PSS from the PEDOT:PSS/rGO composite with respect to PEDOT:PSS. The residual PSS would facilitate adsorption of O_2 on the rGO surface, being favorable for ORR, as reported for the sulfonated hyperbranched poly(ether ketone)-grafted multiwalled C nanotubes.[39] Moreover, Fourier transform infrared spectra of the PEDOT:PSS/rGO composites before and after H_2SO_4 treatment were recorded. The H_2SO_4-treated composite exhibits a weak band near 600 cm^{-1} (Figure S3 in the SI), attributed to the S−O stretching modes of the sulfate ions.[40] This observation suggests that some sulfate ions remain in the composite film even after careful rinsing with ample water.

Electrocatalytic Activity of the PEDOT:PSS/rGO Composites for ORR. The conductivity enhancement of PEDOT as well as electron transfer observed in PEDOT:PSS/rGO would endow PEDOT and rGO with improved electrocatalytic activities for ORR. Cyclic voltammograms (CVs) in an O_2-saturated 0.1 M KOH solution on H_2SO_4-treated PEDOT:PSS, rGO, and PEDOT:PSS/rGO electrodes were collected to evaluate the possibility of these materials as catalysts for ORR (Figure 4a). The CVs of these three catalysts show ORR waves with reduction peaks around −0.43, −0.32, and −0.27 V, respectively. The onset potentials of ORR were read at −0.30, −0.21, and −0.16 V, correspondingly. Notably, the PEDOT:PSS/rGO composite exhibits much higher cathodic current density together with positively shifted onset and peak potentials of ORR with respect to those of the individual components. Linear-sweep voltammograms (LSVs) performed on a rotating disk electrode (RDE) further demonstrated that the H_2SO_4-treated PEDOT:PSS/rGO composite has the most positive onset potential of −0.14 V. The LSV of this H_2SO_4-treated composite also shows the strongest limiting diffusion current at −0.8 V, being about 1.5 times stronger than those of the H_2SO_4-treated PEDOT:PSS and rGO electrodes (Figure 4b). Accordingly, H_2SO_4 post-treatment improved the electrocatalytic performances of the PEDOT:PSS/rGO composite for ORR. This is mainly due to the conductivity increase of PEDOT and the further reduction of rGO by concentrated H_2SO_4 (Figure S4 in the SI), which can further improve the electron-transfer kinetics, exhibiting synergistic enhancement of its electrocatalytic activity.

RDE voltammetry measurements at various rotation rates were performed to explore the mechanism of ORR catalyzed by the H_2SO_4-treated PEDOT:PSS/rGO composite. As shown in Figure 4c, the limiting current density of ORR at the PEDOT:PSS/rGO electrode increases with the rotation rate in the range of 400−2025 rpm, indicating that ORR is controlled by mass diffusion. Moreover, at a given rotation rate, the limiting current density of ORR at the composite electrode is much stronger than those at the electrodes of individual components (Figure S5 in the SI). The Koutecky−Levich (K−L) equation was applied to estimate the transferred electron number per oxygen molecule involved in ORR.[41] It can be seen that the K−L plots (j^{-1} vs $\omega^{-1/2}$) have good linearity for PEDOT:PSS, rGO, and PEDOT:PSS/rGO composite electrodes at various potentials (Figure S6 in the SI and Figure 4d). The electron-transfer number (n) for ORR at the composite electrode was estimated to be 3.3−3.8 at potentials ranging from −0.4 to −0.7 V, always being higher than those at the PEDOT:PSS (2.0−2.2) or rGO (2.3−2.8) electrode (Figure 4e). These results demonstrated that the ORR process at the PEDOT:PSS/rGO composite electrode is nearly a four-electron pathway, whereas a two-electron process dominates the ORR reaction on the PEDOT:PSS or rGO electrode. Rotation ring disk electrode (RRDE) studies were conducted to further validate the ORR pathway by monitoring the intermediate peroxide species of HO_2^- generated at the disk electrode in an alkaline medium during the ORR process. As shown in Figure 4f, all three catalysts generated ring currents over the potential range from −0.2 to −0.8 V for ORR. Notably, both individual components exhibited much stronger ring currents than the composite at −0.8 V. The HO_2^- yields derived from the RRDE results for PEDOT:PSS, rGO, and the composite were 74%, 59%, and 33%, respectively, at a potential of −0.8 V. Accordingly, the electron-transfer numbers (n) were

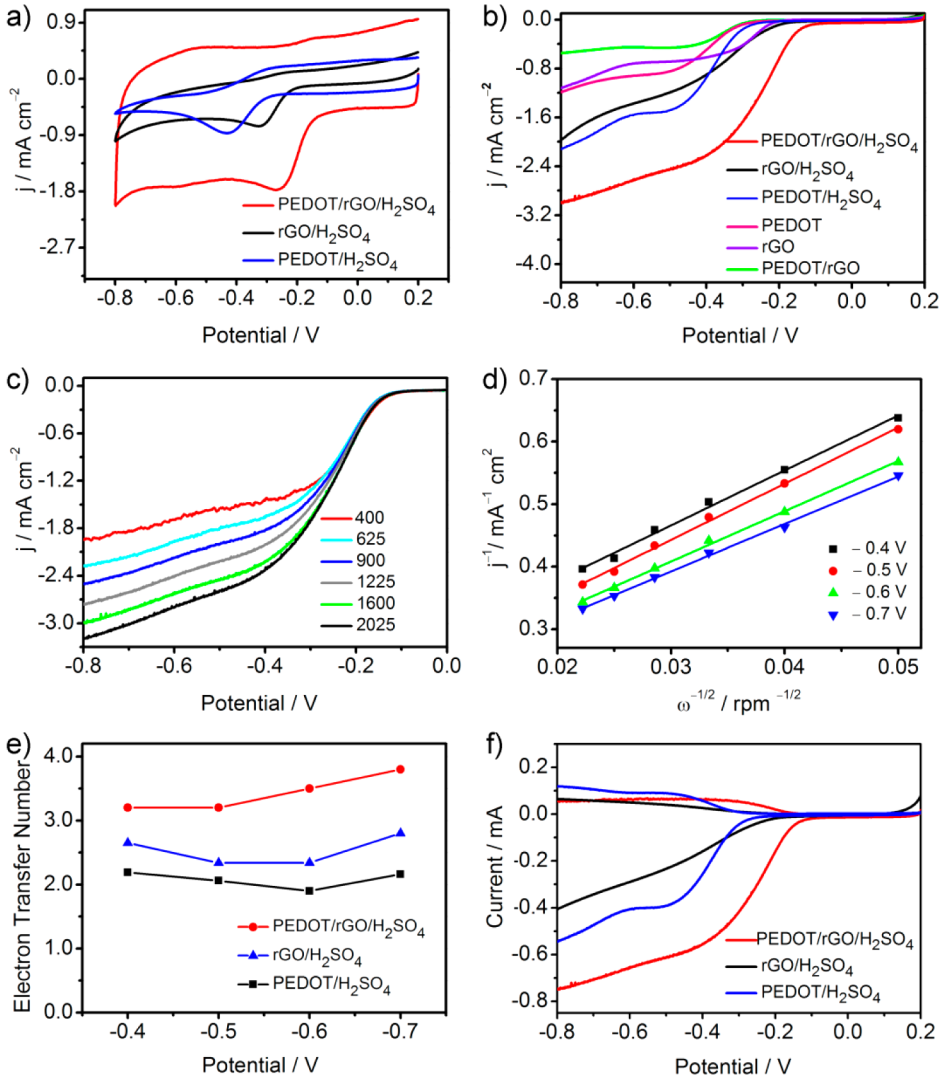

Figure 4. (a) CVs of ORR on H_2SO_4-treated PEDOT:PSS, rGO, and PEDOT:PSS/rGO composites in an O_2-saturated 0.1 mol L^{-1} KOH solution at a scan rate of 100 mV s^{-1}. (b) LSV curves of PEDOT:PSS, rGO, and PEDOT:PSS/rGO composites with and without post-treatment by concentrated H_2SO_4 at 1600 rpm. (c) RDE voltammograms of H_2SO_4-treated PEDOT:PSS/rGO at different rotating rates in an O_2-saturated 0.1 mol L^{-1} KOH solution at a scan rate of 10 mV s^{-1}. (d) K–L plots of j^{-1} versus $\omega^{-1/2}$ obtained from the RDE data at different electrode potentials. (e) Electron-transfer numbers as a function of the overpotential of H_2SO_4-treated PEDOT:PSS, rGO, and PEDOT:PSS/rGO composites. (f) RRDE volatmmograms of H_2SO_4-treated PEDOT:PSS, rGO, and PEDOT:PSS/rGO electrodes in O_2-saturated 0.1 M KOH at 1600 rpm. The ring electrode was polarized at −0.5 V.

measured over the potential range of −0.4 to −0.7 V to be 2.3–2.4 for PEDOT:PSS, 2.7–2.8 for rGO, and 3.1–3.4 for PEDOT:PSS/rGO, being consistent with the RDE results. All of these observations described above reflect the synergistically enhanced electrocatalytic efficiency of the composite catalyst.

The composites with different mass ratios of PEDOT:PSS to rGO (w/w) were prepared to optimize the electrocatalytic performances of the composites for ORR based on RDE measurements (Figures S7–S10 in the SI). It was observed that PEDOT:PSS/rGO (2:1) exhibits a higher ORR cathodic current than the other composites with the highest positive onset potential of −0.14 V. The electron-transfer numbers as a function of the overpotential for the different composites were estimated based on the K–L plots, and PEDOT:PSS/rGO (2:1) has the highest electron-transfer number (3.3–3.8). The dependence of the onset potential, peak current, and electron-transfer number on the mass ratios of PEDOT:PSS to rGO further proves the synergistically enhanced electrochemical activities of PEDOT:PSS and rGO in the composite for ORR.[42]

Durability of the PEDOT:PSS/rGO Composite Catalyst for ORR. Poor fuel tolerance and CO poisoning are critical issues for the Pt-based ORR catalysts. To further verify the remarkable electrocatalytic performances of the composites, chronoamperometric responses for ORR at the PEDOT:PSS/rGO and commercial Pt/C electrodes in the electrolyte containing methanol or CO were illustrated in Figure 5. It is clear that a distinct decrease in the cathodic current was observed for the Pt/C electrode upon the addition of 3 M methanol or 10% CO to the O_2-saturated electrolyte, whereas no obvious interference to the PEDOT:PSS/rGO composite was detected under identical conditions. These results indicate that the composite catalyst has a stronger tolerance to the methanol crossover effect and it is insensitive to CO. The durability of the PEDOT:PSS/rGO composite with respect to commercial Pt/C for ORR was assessed via chronoamper-

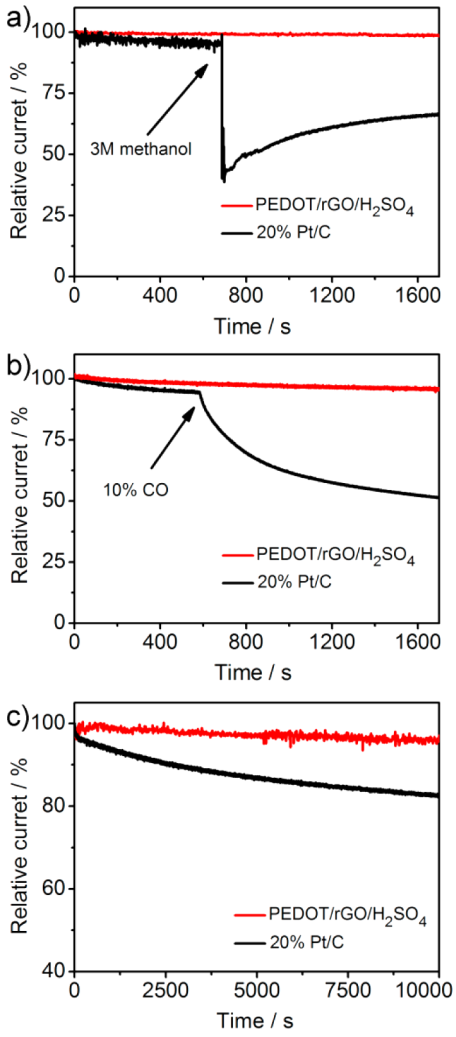

Figure 5. Chronoamperometric responses of H_2SO_4-treated PEDOT:PSS/rGO and Pt/C at −0.5 V in an O_2-saturated 0.1 M KOH solution with a rotation speed of 900 rpm: (a) 3.0 M methanol added; (b) 10% CO added; (c) without additional additives.

omieric tests at −0.5 V in O_2-saturated 0.1 M KOH at a rotation rate of 900 rpm. As revealed in Figure 5c, the composite exhibits very slow attenuation with a high current retention of 95% after 10000 s. In sharp contrast, the commercial Pt/C shows a much faster current decrease with 80% retention, indicating that the PEDOT:PSS/rGO electrocatalyst is much more stable than the commercial Pt/C catalyst.

3. CONCLUSIONS

We have developed a solution-processed method for fabrication of the metal-free ORR electrocatalyst via a simple solution blending of PEDOT:PSS and rGO combined with a facile H_2SO_4 post-treatment process at room temperature. The resultant PEDOT:PSS/rGO composite exhibits synergistically enhanced ORR electrocatalytic activity with a quasi-four-electron pathway, better tolerance to the methanol crossover effect and CO poisoning, and improved durability over that of the Pt/C electrode. We believe that the present findings not only will provide an important clue to developing metal-free ORR catalysts based on the solution assembly of conducting polymers but also can be further extended to develop conducting polymer/rGO composites for other electrochemical applications, such as sensors and energy storage and conversion devices.

4. EXPERIMENTAL SECTION

Synthesis of GO. GO was prepared by the modified Hummers' method.[43] Briefly, graphite powder (325 mesh, 3.0 g) was slowly added to concentrated sulfuric acid (70 mL) in a beaker under constant stirring at room temperature, and then sodium nitrate (1.5 g) was added. The beaker was transferred to an ice bath for cooling to 0 °C under vigorous agitation, and potassium permanganate (9.0 g) was then added slowly to keep the temperature of the suspension lower than 20 °C. Subsequently, the reaction mixture was taken from the ice bath and transferred to a 35−40 °C water bath with stirring for about 0.5 h to form a thick paste. Then 140 mL of water was dripped into the mixture, and the solution was stirred for another 15 min. An additional 500 mL of water and 15 mL of H_2O_2 (30% aqueous solution) were added to terminate the reaction, turning the solution from brown to yellow. The solution was filtered and washed with a 1:10 HCl aqueous solution to remove metal ions followed by washing with ample water to remove the residual acid. The resultant solid was then dispersed in distilled water under an ultrasonication bath to make a GO aqueous suspension. The obtained GO was purified by repeated centrifugation at 4000 rpm and then dialysis for 1 week to remove graphite oxide particles and the residual metal species. The final pure aqueous GO was diluted to the desired concentration for subsequent applications.

Synthesis of rGO. rGO was prepared under alkaline conditions according to the reported method.[44] Briefly, the as-prepared GO was diluted by distilled water to 1 mg mL^{-1}. A total of 100 mL of a yellow-brown GO suspension (1 mg mL^{-1}) mixed with a 1 mL KOH solution (8 M) was poured into a serum bottle. Then, the solution was submitted to a mild sonication (25 W, 40 kHz) at a constant temperature of 80 °C for 6 h. The resultant black suspension was purified by repeated centrifugation and washing with distilled water to obtain rGO for subsequent characterization.

Preparation of the Electrodes. A total of 10 μL of the PEDOT:PSS/rGO mixed solution (1 mg mL^{-1}) with a given composition was drop-casted onto a glassy carbon (GC) electrode and dried under room temperature. Then the as-prepared modified electrodes were treated with concentrated H_2SO_4 for 1 h. Subsequently, the electrodes were rinsed with deionized water to remove H_2SO_4 and dried under ambient conditions. For RDE and RRDE voltammograms, 30 μL of the mixed solution was drop-casted onto the surface of the disk electrode (disk area = 0.25 cm^2 and ring area = 0.19 cm^2) followed by the treatments outlined above.

Characterizations. TEM images were collected on a H-76501B (Hitachi) transmission electron microscope. AFM images were obtained using a Nanoscope III MultiMode SPM (Digital Instruments). XPS was performed using an ESCALAB 250 photoelectron spectrometer (ThermoFisher Scientific) with Al Kα (1486.6 eV) as the X-ray source set at 150 W and a pass energy of 30 eV for a high-resolution scan. Raman spectra were recorded on a RM 2000Microscopic confocal Raman spectrometer (Renishaw PLC, England) using a 514 nm laser beam. The electrical conductivities were measured using a four-probe conductivity test meter (KDY-1, Kunde Technology Co., Ltd.) at room temperature.

Electrochemical Measurements. Electrochemical measurements were carried out in a typical three-electrode cell on a potentiostat (CHI 760D, CH instrument, Inc.) using a Pt wire as the counter electrode and Ag/AgCl (KCl saturated) as the counter electrode. The catalyst-modified GC electrode was used as the working electrode with a 0.1 M KOH aqueous solution as the electrolyte for ORR. The electrolyte solution was bubbled with N_2 or O_2 for 30 min before each measurement to ensure that the solution was O_2-free or saturated and kept bubbling throughout the tests. RDE or RRDE voltammetry was performed on a MSRX electrode rotator (Pine Instrument) coupled with a CHI 760D potentiostat at a scan rate of 10 mV s^{-1}.

■ ASSOCIATED CONTENT

Supporting Information

Calculation methods for the kinetic parameters of ORR, conductivities of PEDOT:PSS and the PEDOT:PSS/rGO composite, S 2p XPS spectra of PEDOT:PSS, C 1s XPS spectra of rGO before and after H_2SO_4 treatment, RDE voltammograms for ORR on H_2SO_4-treated PEDOT:PSS, rGO, and PEDOT:PSS/rGO composites (5:1, 1:1, and 1:2, w/w), K−L plots of ORR on H_2SO_4-treated PEDOT:PSS, rGO, and PEDOT:PSS/rGO composites (5:1, 1:1, and 1:2, w/w) at different electrode potentials, and electron-transfer numbers as a function of the overpotential of the composites with different mass ratios of PEDOT:PSS to rGO (w/w). This material is available free of charge via the Internet at http://pubs.acs.org.

■ AUTHOR INFORMATION

Corresponding Author

*E-mail: chunli@mail.tsinghua.edu.cn.

Author Contributions

The manuscript was written through contributions of all authors. All authors have given approval to the final version of the manuscript.

Notes

The authors declare no competing financial interest.

■ ACKNOWLEDGMENTS

This work was supported by the National Basic Research Program of China (Grant 2012CB933402) and Natural Science Foundation of China (Grants 21274074 and 51161120361).

■ REFERENCES

(1) Markovic, N. M.; Schmidt, T. J.; Stamenkovic, V.; Ross, P. N. Oxygen Reduction Reaction on Pt and Pt Bimetallic Surfaces: A Selective Review. *Fuel Cells* **2001**, *1*, 105−116.

(2) Gewirth, A. A.; Thorum, M. S. Electroreduction of Dioxygen for Fuel-Cell Applications: Materials and Challenges. *Inorg. Chem.* **2010**, *49*, 3557−3566.

(3) Bing, Y.; Liu, H.; Zhang, L.; Ghosh, D.; Zhang, J. Nanostructured Pt-Alloy Electrocatalysts for PEM Fuel Cell Oxygen Reduction Reaction. *Chem. Soc. Rev.* **2010**, *39*, 2184−2202.

(4) Debe, M. K. Electrocatalyst Approaches and Challenges for Automotive Fuel Cells. *Nature* **2012**, *486*, 43−51.

(5) Bruce, P. G.; Freunberger, S. A.; Hardwick, L. J. Li−O_2 and Li−S batteries with high energy storage. *Nat. Mater.* **2012**, *11*, 19−29.

(6) Cao, R.; Lee, J.-S.; Liu, M.; Cho, J. Recent Progress in Non-Precious Catalysts for Metal−Air Batteries. *Adv. Energy Mater.* **2012**, *2*, 816−829.

(7) Cheng, F.; Chen, J. Metal−Air Batteries: From Oxygen Reduction Electrochemistry to Cathode Catalysts. *Chem. Soc. Rev.* **2012**, *41*, 2172−2192.

(8) Wang, C.; Markovic, N. M.; Stamenkovic, V. R. Advanced Platinum Alloy Electrocatalysts for the Oxygen Reduction Reaction. *ACS Catal.* **2012**, *2*, 891−898.

(9) Wu, J.; Yang, H. Platinum-Based Oxygen Reduction Electrocatalysts. *Acc. Chem. Res.* **2013**, *46*, 1848−1857.

(10) Porter, N. S.; Wu, H.; Quan, Z. Shape-Control and Electrocatalytic Activity-Enhancement of Pt-Based Bimetallic Nanocrystals. *Acc. Chem. Soc.* **2013**, *46*, 1867−1877.

(11) Winther-Jensen, B.; MacFarlane, D. R. New Generation, Metal-Free Electrocatalysts for Fuel Cells, Solar Cells and Water Splitting. *Energy Environ. Sci.* **2011**, *4*, 2790−2798.

(12) Yuan, X.; Ding, X.-L.; Wang, C.-Y.; Ma, Z.-F. Use of Polypyrrole in Catalysts for Low Temperature Fuel Cells. *Energy Environ. Sci.* **2013**, *6*, 1105−1124.

(13) Wang, H.; Maiyalagan, T.; Wang, X. Review on Recent Progress in Nitrogen-Doped Graphene: Synthesis, Characterization, and Its Potential Applications. *ACS Catal.* **2012**, *2*, 781−794.

(14) Zheng, Y.; Jiao, Y.; Jaroniec, M.; Jin, Y.; Qiao, S. Z. Nanostructured Metal-Free Electrochemical Catalysts for Highly Efficient Oxygen Reduction. *Small* **2012**, *8*, 3550−3566.

(15) Yang, Z.; Nie, H.; Chen, X.; Chen, X.; Huang, S. Recent Progress in Doped Carbon Nanomaterials as Effective Cathode Catalysts for Fuel Cell Oxygen Reduction Reaction. *J. Power Sources* **2013**, *236*, 238−249.

(16) Paraknowitsch, J. P.; Thomas, A. Doping Carbons Beyond Nitrogen: An Overview of Advanced Heteroatom Doped Carbons with Boron, Sulphur and Phosphorus for Energy. *Energy Environ. Sci.* **2013**, *6*, 2839−2855.

(17) Dai, L.; Chang, D. W.; Baek, J.-B.; Lu, W. Carbon Nanomaterials for Advanced Energy Conversion and Storage. *Small* **2012**, *8*, 1130−1166.

(18) Dai, L. Functionalization of Graphene for Efficient Energy Conversion and Storage. *Acc. Chem. Res.* **2013**, *46*, 31−42.

(19) Sun, Y.; Wu, Q.; Shi, G. Graphene Based New Energy Materials. *Energy Environ. Sci.* **2011**, *4*, 1113−1132.

(20) Huang, C.; Li, C.; Shi, G. Graphene Based Catalysts. *Energy Environ. Sci.* **2012**, *5*, 8848−8868.

(21) Su, D. S.; Perathoner, S.; Centi, G. Nanocarbons for the Development of Advanced Catalysts. *Chem. Rev.* **2013**, *113*, 5782−5816.

(22) Winther-Jensen, B.; Winther-Jensen, O.; Forsyth, M.; MacFarlane, D. R. High Rates of Oxygen Reduction over a Vapor Phase−Polymerized PEDOT Electrode. *Science* **2008**, *321*, 671−674.

(23) Gong, K.; Du, F.; Xia, Z.; Durstock, M.; Dai, L. Nitrogen-Doped Carbon Nanotube Arrays with High Electrocatalytic Activity for Oxygen Reduction. *Science* **2009**, *323*, 760−764.

(24) Qu, L.; Liu, Y.; Baek, J.-B.; Dai, L. Nitrogen-Doped Graphene as Efficient Metal-Free Electrocatalyst for Oxygen Reduction in Fuel Cells. *ACS Nano* **2010**, *4*, 1321−1326.

(25) Sun, Y.; Li, C.; Xu, Y.; Bai, H.; Yao, Z.; Shi, G. Chemically Converted Graphene as Substrate for Immobilizing and Enhancing the Activity of a Polymeric Catalyst. *Chem. Commun.* **2010**, *46*, 4740−4742.

(26) Chen, J.; Zhao, L.; Bai, H.; Shi, G. Electrochemical Detection of Dioxygen and Hydrogen Peroxide by Hemin Immobilized on Chemically Converted Graphene. *J. Electroanal. Chem.* **2011**, *657*, 34−38.

(27) Sun, Y.; Li, C.; Shi, G. Nanoporous Nitrogen Doped Carbon Modified Graphene as Electrocatalyst for Oxygen Reduction Reaction. *J. Mater. Chem.* **2012**, *22*, 12810−12816.

(28) Hong, W.; Xu, Y.; Lu, G.; Li, C.; Shi, G. Transparent Graphene/PEDOT−PSS Composite Films as Counter Electrodes of Dye-Sensitized Solar Cells. *Electrochem. Commun.* **2008**, *10*, 1555−1558.

(29) Tung, V. C.; Kim, J.; Cote, L. J.; Huang, J. Sticky Interconnect for Solution-Processed Tandem Solar Cells. *J. Am. Chem. Soc.* **2011**, *133*, 9262−9265.

(30) Kim, G. H.; Hwang, D. H.; Woo, S. I. Thermoelectric Properties of Nanocomposite Thin Films Prepared with Poly(3,4-ethylenedioxythiophene) Poly(styrenesulfonate) and Graphene. *Phys. Chem. Chem. Phys.* **2012**, *14*, 3530−3536.

(31) Xia, Y.; Ouyang, J. Significant Conductivity Enhancement of Conductive Poly(3,4-ethylenedioxythiophene):Poly(styrenesulfonate) Films through a Treatment with Organic Carboxylic Acids and Inorganic Acids. *ACS Appl. Mater. Interfaces* **2010**, *2*, 474−483.

(32) Xia, Y.; Sun, K.; Ouyang, J. Solution-Processed Metallic Conducting Polymer Films as Transparent Electrode of Optoelectronic Devices. *Adv. Mater.* **2012**, *24*, 2436−2440.

(33) Wang, S.; Yu, D.; Dai, L. Polyelectrolyte Functionalized Carbon Nanotubes as Efficient Metal-free Electrocatalysts for Oxygen Reduction. *J. Am. Chem. Soc.* **2011**, *133*, 5182−5186.

(34) Wang, S.; Yu, D.; Dai, L.; Chang, D. W.; Baek, J.-B. Polyelectrolyte-Functionalized Graphene as Metal-Free Electrocatalysts for Oxygen Reduction. *ACS Nano* **2011**, *5*, 6202−6209.

(35) Garreau, S.; Louarn, G.; Buisson, J. P.; Froyer, G.; Lefrant, S. In Situ Spectroelectrochemical Raman Studies of Poly(3,4-ethylenedioxythiophene) (PEDT). *Macromolecules* **1999**, *32*, 6807−6812.
(36) Ouyang, J.; Xu, Q.; Chu, C.-W.; Yang, Y.; Li, G.; Shinar, J. On the Mechanism of Conductivity Enhancement in Poly(3,4-ethylenedioxythiophene):Poly(styrene sulfonate) Film through Solvent Treatment. *Polymer* **2004**, *45*, 8443−8450.
(37) Ferrari, A. C.; Meyer, J. C.; Scardaci, V.; Casiraghi, C.; Lazzeri, M.; Mauri, F.; Piscanec, S.; Jiang, D.; Novoselov, K. S.; Roth, S.; Geim, A. K. Raman Spectrum of Graphene and Graphene Layers. *Phys. Rev. Lett.* **2006**, *97*, 187401.
(38) Ferrari, A. C. Raman Spectroscopy of Graphene and Graphite: Disorder, Electron−Phonon Coupling, Doping and Nonadiabatic Effects. *Solid State Commun.* **2007**, *143*, 47−57.
(39) Sohn, G.-J.; Choi, H.-J.; Jeon, I.-Y.; Chang, D. W.; Dai, L.; Baek, J.-B. Water-Dispersible, Sulfonated Hyperbranched Poly(ether-ketone) Grafted Multiwalled Carbon Nanotubes as Oxygen Reduction Catalysts. *ACS Nano* **2012**, *6*, 6345−6355.
(40) Givan, A.; Larsen, L. A.; Loewenschuss, A.; Nielsen, C. J. Matrix isolation mid- and far-infrared spectra of sulfuric acid and deuterated sulfuric acid vapors. *J. Mol. Struct.* **1999**, *509*, 35−47.
(41) Chen, W.; Chen, S. Oxygen Electroreduction Catalyzed by Gold Nanoclusters: Strong Core Size Effects. *Angew. Chem., Int. Ed.* **2009**, *48*, 4386−4389.
(42) Chen, P.; Xiao, T.-Y.; Qian, Y.-H.; Li, S.-S.; Yu, S.-H. A Nitrogen-Doped Graphene/Carbon Nanotube Nanocomposite with Synergistically Enhanced Electrochemical Activity. *Adv. Mater.* **2013**, *25*, 3192−3196.
(43) Xu, Y.; Bai, H.; Lu, G.; Li, C.; Shi, G. Flexible Graphene Films via the Filtration of Water-Soluble Noncovalent Functionalized Graphene Sheets. *J. Am. Chem. Soc.* **2008**, *130*, 5856−5857.
(44) Fan, X.; Peng, W.; Li, Y.; Li, X.; Wang, S.; Zhang, G.; Zhang, F. Deoxygenation of Exfoliated Graphite Oxide under Alkaline Conditions: A Green Route to Graphene Preparation. *Adv. Mater.* **2008**, *20*, 4490−4493.